Plasma Sources Sci. Technol.

Characterization of injected aluminum oxide nanoparticle clouds in an rf discharge

Harald Krüger[1], Carsten Killer[2], Stefan Schütt[1] and André Melzer[1]

[1] Ernst-Moritz-Arndt-Universität Greifswald, 17489 Greifswald, Germany
[2] Max-Planck-Institut für Plasmaphysik, 17491 Greifswald, Germany

E-mail: harald.krueger@physik.uni-greifswald.de

Abstract. An experimental setup to deagglomerate and insert nanoparticles into a radio frequency (rf) discharge has been developed to confine defined aluminum oxide nanoparticles in a dusty plasma. For the confined particle clouds we have measured the spatially resolved in situ size and density distributions. Implementing the whole plasma chamber into the sample volume of an FTIR spectrometer the infrared spectrum of the confined aluminum oxide nanoparticles has been obtained. We have investigated the dependency of the absorbance of the nanoparticles in terms of plasma power, pressure and cloud shape. The particles' infrared phonon resonance has been identified.

1. Introduction

Dusty plasmas have attracted great interest since the first observation of Coulomb crystals in 1994 [1–3]. These plasmas consist, like usual plasmas, of electrons, ions and neutral gas atoms, and in addition of particles with sizes in the range of a few nanometers to up to tens of micrometers. In the plasma, particles acquire a high (negative) charge due to the inflow of plasma electrons and ions. With these properties, the topic has had a significant influence on the research of technical plasma processes and astrophysics.

The field of dusty plasmas has developed for many years by investigations on micrometer sized particles. This is also due to the comparatively easy way to insert microparticles into the plasma by dust shakers [3]. Plasmas with embedded submicrometer or nanometer sized dust have become a research field of interest for fundamental questions including magnetized dusty plasmas or charge-depletion effects [4–7]. In this article, we will use the term nanodust for particles of about 100 nm radius and below. To inject externally produced well-characterized nanoparticles dust shakers, however, do not suit the needs. Nanoparticles have the habit to agglomerate to larger clusters under typical conditions. This results in clogging up the shaker sieves by the agglomerates and not inserting any particles into the discharge. Using larger meshes, agglomerates are inserted into the discharge without disaggregation. For these nanoparticle agglomerates repulsive Coulomb forces due to charging in the plasma are usually not sufficient to overcome the van-der-Waals sticking interaction.

An alternative approach is the formation of nanoparticles inside the plasma. One possibility is to grow particles in a reactive gas. This is mainly put into effect by adding a reactive gas species to the background gas. The particles grow by chemical pathways and typically build a dust cloud of monodisperse nanoparticles inside the plasma [4, 5, 8, 9]. However, for particle forming discharges a time-resolved monitoring of the particle size is required. Also, particle properties might change during particle growth [10, 11].

Inserting externally produced particles usually has the advantage that some material properties are already known. This applies especially for the refractive index and particle sizes given by the manufacturer. However, due to typically polydisperse nanoparticle mixtures, it is necessary to measure the particle size distribution of the particles trapped in the discharge in situ. Such distributions have been determined by Mie ellipsometry [10–14] and by angular resolved Mie scattering measurements [15, 16].

Besides the size, the particle number density is important to characterize the dusty plasma. Absorption measurements allow to measure the spatially resolved dust density inside the plasma. For dusty plasmas with grown nanoparticles the density is usually so high that nearly all electrons are bound to the particles leading to strong electron depletion effects [17–19]. This way, the nanodusty plasma becomes a dusty plasma of mainly positively charged ions and negatively charged nanoparticles. Hence, for a quantitative description it becomes necessary to measure the particle charge in situ. One way to determine the particle charge in this situation is to analyze the propagation of dust-density waves through the nanodusty plasma [18]. In absence of dust-density waves other techniques are required. As an alternative approach one could use the dust particles' phonon resonance in the infrared spectral range. As an example, for aluminum oxide particles the phonon resonance is expected to shift by about $\Delta\lambda^{-1} = 4\,\mathrm{cm}^{-1}$ for nanoparticles of 50 nm radius under typical plasma conditions [20, 21].

Hence, to further explore nanodusty plasmas for magnetization or charge-depletion effects it is necessary to combine techniques for reproducibly inserting externally produced nanoparticles into a plasma and methods to characterize the cloud of trapped nanoparticles with respect to size, density and charge (distributions). In this article we describe a dust injection setup to insert and confine nearly monodisperse nanoparticle clouds. To characterize these particles concerning size and density distribution we will use optical in situ Mie-scattering techniques. Afterwards, we will investigate the in situ IR absorption spectra of the trapped nanoparticles. The mentioned phonon resonance in the infrared spectral range will be measured at the given dust density with an FTIR spectrometer as a prerequisite to apply this technique as a charge diagnostic in the future.

2. Experiment

The main experiments have been performed in a symmetric, capacitively coupled radio frequency (rf) plasma discharge in a modified version of an IMPF (K2) chamber [22], see Fig. 1a). Two different vessel walls have been used for the experiments: a glass ring with full 360° optical access for size and density measurements and a metal body with a fourfold optical access for the integration into an FTIR spectrometer. In all cases, the electrodes have a diameter of 80 mm and a distance of 30 mm. The plasma is ignited with an rf voltage at 13.56 MHz at an argon gas pressure of the order of 10 Pa and at low plasma powers in the range of 1 to 10 W in push-pull mode. According to Klindworth *et al* [23], who have performed Langmuir probe measurements in essentially the same chamber,

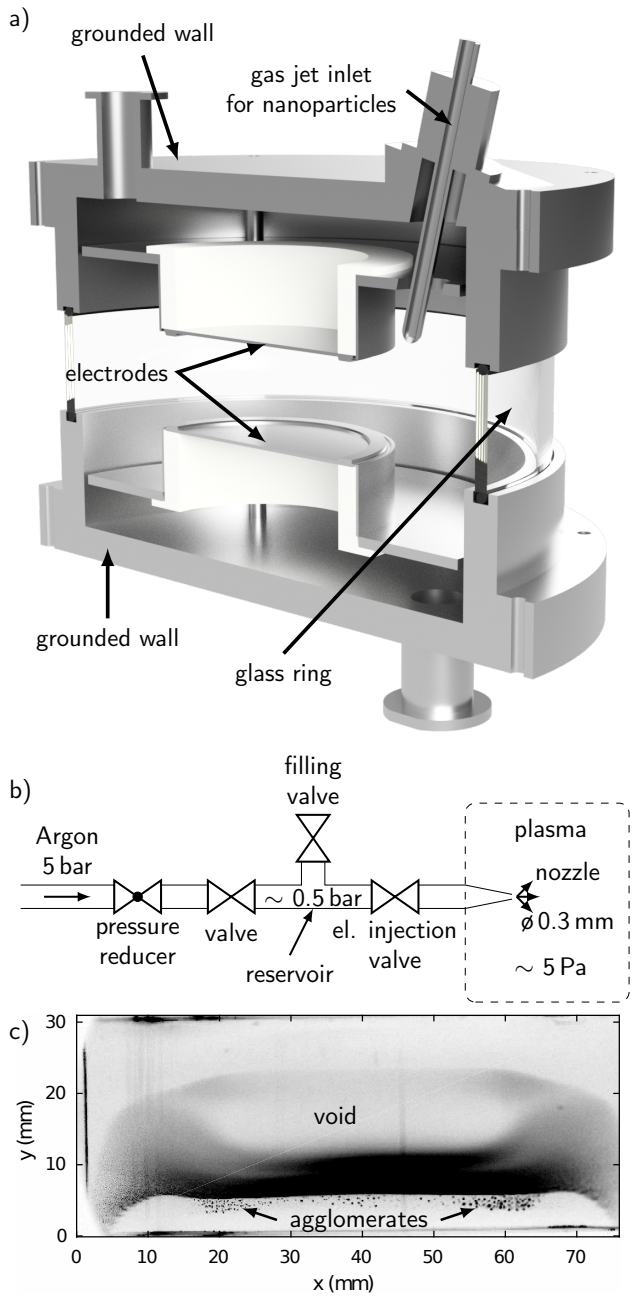

Figure 1. a) Modified IMPF (K2) chamber with a borosilicate glass ring as a wall. The chamber consits of two electrodes with a diameter of 80 mm and a distance of 30 mm, upper and lower bases with gas inlets and a dust injection nozzle. b) Sketch of the nanoparticle injection setup consisting of a small particle reservoir flooded with argon at ~ 0.5 bar, electric injection valve and a nozzle with an opening diameter of 0.3 mm. c) Inverted snapshot of the scattered light from the central cross section of a laser-illuminated dust cloud.

the electron temperature is about $T_e \approx 3\,\mathrm{eV}$, the electron and ion density $n_{e,i} \approx 6.5 \times 10^{14}\,\mathrm{m}^{-3}$ and the plasma potential $\phi_p \approx 36\,\mathrm{V}$ in the dust-free plasma. The electron temperature is found to increase and the ion density to decrease in the dust cloud [22].

A gas jet has been developed to add commercially available nanodust material to the plasma [24, 25]. In the experiments described here, we use aluminum oxide (Al_2O_3) particles from Goodfellow with a nominal size of less than 100 nm. As one can see from both magnifications in the scanning electron microscope (SEM) images in Fig. 2a), one finds a wide range of particle sizes. There is a large number of submicron particles. Under usual conditions these small particles can stick together to form large polydisperse agglomerates in the micrometer range.

The main idea behind the gas jet setup is to shoot the material with an argon gas jet through a small nozzle into the discharge, see Fig. 1b). The dust material is put into a small reservoir through a filling valve. Opening an electric injection valve evacuates the small volume in the beginning. Here, only a small part of the nanoparticles leaves the reservoir. Afterwards, the reservoir is flooded by argon using a pressure reducer and valve. The gas pressure in the small volume then is in the range of 0.5 bar. Opening the injection valve blows the particles through a small nozzle with an orifice of 0.3 mm diameter into the plasma where the gas pressure is about $p = 10\,\mathrm{Pa}$. The huge pressure difference between the reservoir and the plasma chamber disperses the agglomerated particles in the plasma volume. The volume of the reservoir is small enough, so that a single gas shot is not sufficient to extinguish the plasma. During a shot the gas pressure in the plasma chamber briefly jumps to a maximum value of about 100 Pa where the plasma still can be sustained. The gas shot can be repeated several times until the desired filling of the plasma with dust is achieved.

Other means of dust insertion (e.g. by shakers) were unsuccessful in generating clouds of nanoparticles. Further, the gas jet injection has the advantage to insert a large variety of possible materials with known characteristics, like the refractive index.

The trapped dust cloud is then characterized by Mie-scattering and tomography for size and density distributions. The phonon spectra of the dust is recorded using an FTIR spectrometer as described below.

3. Results

3.1. Qualitative impression

The commercially available aluminum oxide particles have been injected by our gas jet. A confined cloud of

particles can be observed inside the plasma chamber instantly. Figure 1c) shows an inverted video snapshot of the area between both electrodes with the confined particle cloud. A laser illuminates a thin slice of the particles, and the scattered laser light is detected by the camera under 90 degrees.

Vertically, the cloud fills about 2/3 of the 30 mm gap between both electrodes, horizontally, the cloud extends over the entire electrode area. In the center of the cloud we can see a nearly particle free area, the so called void [26–31]. Underneath the void there is an area with a huge scattering intensity in comparison to the areas next to and above the void which already hints at a high particle density there. The upper areas seem to be far less populated than those below the void. The dust cloud shows the typical shape of a nanoparticle cloud confined under gravity. A few larger agglomerates can be seen in the sheath as small dots in the lower third of the discharge. There, in the sheath, the particles are trapped due to the dominant action of the gravitational force. These larger particles were not of interest here, since their density is too low for sufficient IR absorption. So they have not been further considered (sometimes, we also got rid of these particles by switching the plasma power off for a very short time).

These first results qualitatively confirm the successful insertion of mainly nanoparticles into an rf discharge by the gas jet injection setup. To support this, we show SEM micrographs of the aluminum oxide particles [see Fig. 2b)], that have been collected from the trapped dust cloud in the discharge by applying a voltage to a holder. The micrographs of the material collected on the holder show particles of about 100 nm radius. These particles are roughly spherical, but might also consist of agglomerates of even smaller particles. Concluding, using our gas jet injection, we are able to confine a dust cloud of mainly nanoparticles of about 100 nm radius in the plasma.

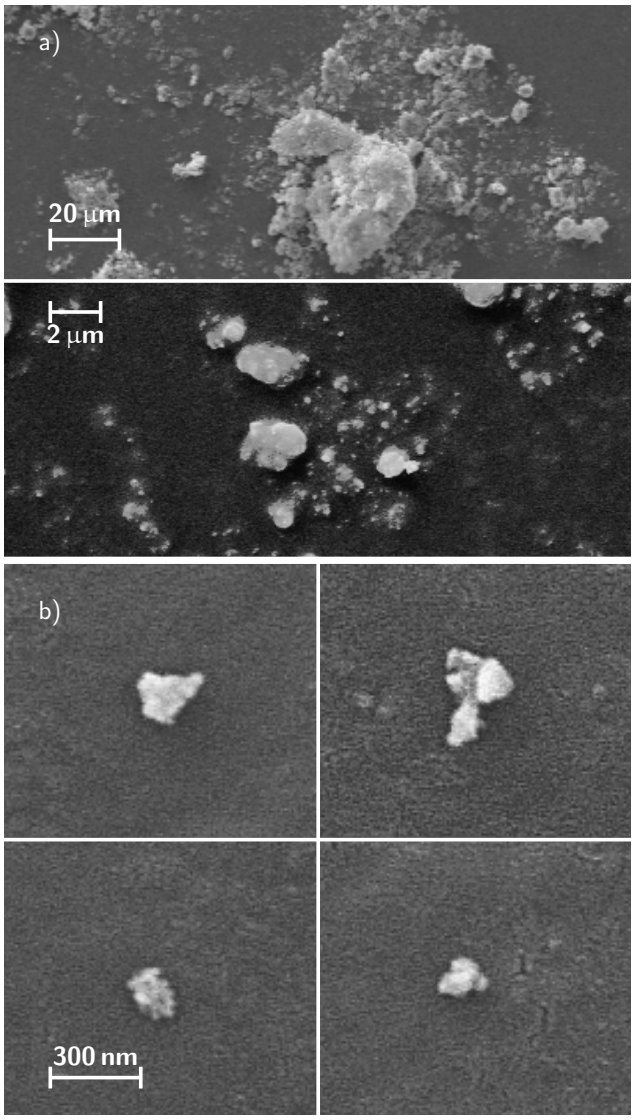

Figure 2. SEM micrographs of a) the original polydisperse aluminum oxide particles at different magnifications and b) aluminum oxide nanoparticles extracted from the dust cloud, confined in a plasma.

3.2. Size measurements

To quantitively analyze the trapped dust cloud we now investigate the particle size distribution by Mie scattering and the density distribution by extinction measurements.

The characteristic angular dependence of the Mie scattering signal for particles in the micrometer range has been used to measure the particle size for single particles [15] and later for large particle clouds [16]. For micron sized particles with the radius a and a light source with the wavelength λ the scattering parameter a/λ is of the order of 10 indicating the Mie regime of scattering where the angular dependent scattering intensity exhibits a sequence of many maxima and minima [34]. The angular scattering dependence differs for nanoparticles. There, $a/\lambda < 1$ indicating quite featureless Rayleigh scattering. One can see in Fig. 3b) that for nanoparticles the angular resolved scattering intensity only has a single characteristic minimum. However, for particles of the order of 100 nm a clear shift of the scattering angle where this minimum occurs can be seen. Hence, this scattering feature can be used for size diagnostics.

The measurement of the angular resolved scattering intensity is carried out in the plasma chamber with the glass ring shown in Fig. 1a). This allows the observation from a wide angular range. A CCD camera with a telecentric lens is mounted on a rotating plate centered around the center of the plasma discharge, see Fig. 3a). The CCD camera is equipped with an op-

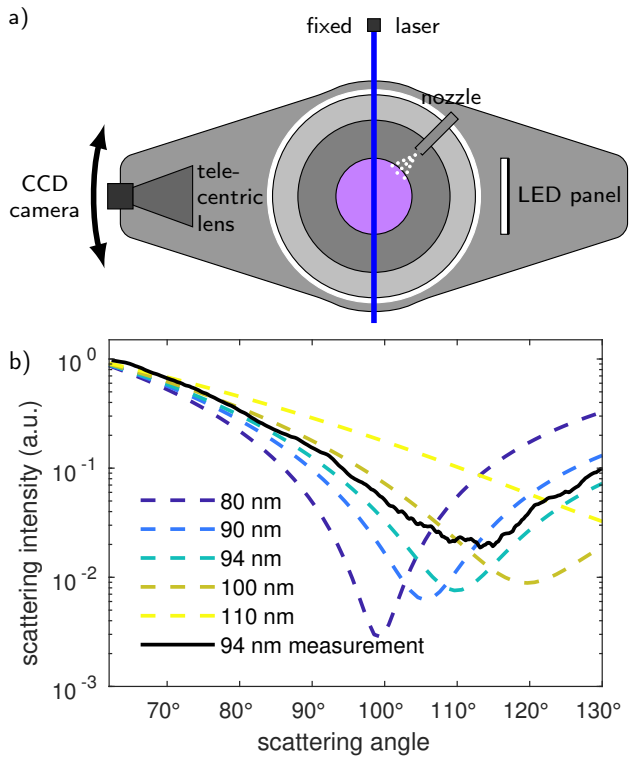

Figure 3. a) Sketch of the size and density diagnostics setup. Size measurements are carried out with the rotatable CCD camera, a telecentric lens and the fixed and widened laser beam. Density measurements use the same rotatable CCD camera and lens, and an opposing white LED panel. b) Calculated parallel polarized scattering intensity on a logarithmic scale over the scattering angle for light with $\lambda = 457\,\mathrm{nm}$ on Al_2O_3 particles of different radii (refractive index of $n = 1.79{+}1.39{\times}10^{-7}\mathrm{i}$) [32,33]. The solid line denotes a measurement for a particular position within the dust cloud.

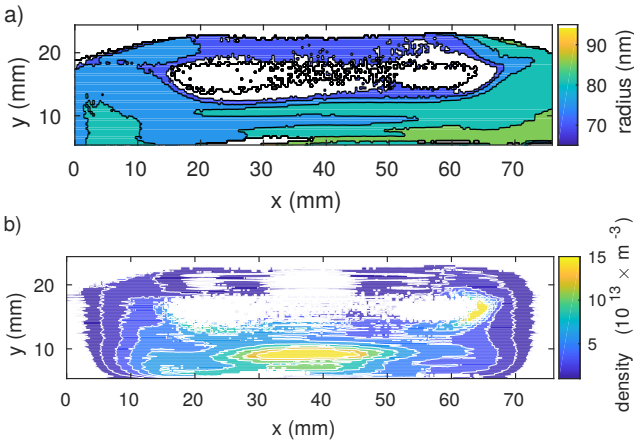

Figure 4. Spatially resolved dust a) size and b) density distribution of the confined nanoparticle cloud. See text for details.

tical filter to suppress the plasma light emission. A vertically expanded blue laser beam illuminates one vertical slize of the dust cloud in the middle of the discharge (details in [35]). The blue illumination laser at $\lambda = 457\,\mathrm{nm}$ is emitting light which is linearly polarized in the horizontal (scattering) plane. Due to the use of aluminum oxide nanoparticles with a nominal size of less than 100 nm as given by the manufacturer a scattering minimum is expected between 90° and 140°. Hence, we recorded scattering signals in the angular range between 60° and 140° relative to the illuminated laser slice. The refractive index of Al_2O_3 has been assumed according to [36] as $n = 1.79 + 1.39 \times 10^{-7}\mathrm{i}$. In analogy to [16], the radius is determined from the comparison of the measured angular resolved scattering intensity with the calculated. The radius is the only free parameter of the Mie scattering problem and is determined by fitting the Mie theory to the measured angular resolved scattering intensities with a least-square fit. This is shown for a certain pixel of the image in Fig. 3b) retrieving a particle radius of 94 nm. This procedure has been repeated for each pixel of the image.

The resulting radii are shown spatially resolved in Fig. 4a). The measured size distribution ranges from small particles of $a = 60\,\mathrm{nm}$ up to $a = 90\,\mathrm{nm}$. While the smaller particles preferably arrange around the void and in the upper part of the cloud, larger particles are located in the lower part and the outer regions of the dust cloud. This vertical separation of sizes and also the vertical asymmetry seems to arise from the small, but still present gravitational force or other slight asymmetries in the trapping conditions (gas flow, electric connections etc.).

The white areas indicate regions with no or just very small particle population which provide insufficient scattering signal for size fitting.

Although the used particle sample is polydisperse, the measurements still confirm the size information by the manufacturer ($a < 100\,\mathrm{nm}$). It is further seen that with our injection system described in Sec. 2 we are able to confine nanoparticle clouds with a quite narrow size range.

3.3. Particle density distribution

Extinction measurements are carried out to determine the density of nanoparticles in the dust cloud. For that purpose a similar setup as for the angular resolved Mie scattering experiments is used. Instead of a stationary laser illumination a homogeneous white LED panel is placed on the other side of the chamber, opposite to the CCD camera to trans-illuminate the particle cloud as in the experiments of Killer *et al* [35, 37]. The extinction of the white light by the dust cloud is measured by the camera. Figure 3a) also shows the setup for the density measurements.

According to the Beer-Lambert law

$$I = I_0 \exp\left(-n_\mathrm{d}\sigma l\right), \qquad (1)$$

we can now obtain information about the particle density n_d by the recorded transmission intensity of the plasma with the particle cloud I and the background plasma transmission intensity without dust particles I_0. Here, σ is the extinction coefficient and l is the length of the extinction path through the dust cloud. Under the assumption of a cylindrically symmetric dust cloud, the radial dust distribution can be calculated from the measured extinction $(I - I_0)/I_0$ by Abel inversion. This calculation is based on an Abel inversion algorithm by Pretzler [38], which has been used by Killer *et al* [35, 37] for dust density measurements with injected microparticles and grown nanoparticles and has been integrated into a MatLab implementation [39] available online. To confirm the cylindrically symmetric shape of the cloud, the measurements are also performed under various angles.

In contrast to the experiments of Killer *et al* [35,37], we now have a wider particle size distribution. We therefore had to account here for a size-dependent scattering cross section σ in evaluating the density from Eq. (1) using the size information of Fig. 4. Taking the size distribution into account is very important for a quantitative determination of the particle densities.

To calculate the density $n_\mathrm{d}(r, z)$, we have to determine the spatially resolved extinction coefficient $\sigma(r, z)$. The extinction coefficient is depending on the size of the particles, the known refractive index n and the wavelength of the incident light of the LED panel. Hence, we take the measured sizes of the particles $a(r, z)$ to calculate the spatially resolved extinction coefficient $\sigma(a(r, z), \lambda)$. The wavelength range of the incident light is determined by the filter in front of the camera lens. For the tomography only light in the range between 440 nm and 560 nm is recorded. There, the dependence of σ on the wavelength is so weak that we can use a wavelength-averaged cross section. We account, however, for the spatial distribution of the particle sizes.

Hence, we get the spatially resolved dust density distribution from (1) shown in Fig. 4b). The void as a nearly particle free area can be clearly seen in the center of the dust cloud. There, the density is lower than $10^{13}\,\mathrm{m}^{-3}$ in comparison to the maximum density of $1.5 \times 10^{14}\,\mathrm{m}^{-3}$ in the central region below the void. This very dense area has already been seen by the high scattering intensity in Fig. 1c). The parts of the cloud that are next to the void are a lot less populated with densities of $2.5 - 5 \times 10^{13}\,\mathrm{m}^{-3}$. Nevertheless, the edge of the void can very clearly be seen due to a higher density at the boundary.

In comparison to other experiments with larger particles in the micrometer range and densities of the order of $10^{11}\,\mathrm{m}^{-3}$ [35], the density in this nanoparticle cloud is by magnitudes larger. In absorption experiments with grown nanoparticles of particle radius $a = 210\,\mathrm{nm}$ [37] a particle density of $2 \times 10^{13}\,\mathrm{m}^{-3}$ has been obtained. In other experiments with particle radii of $a = 200\,\mathrm{nm}$, where the dust density has been measured via laser light absorption, Tadsen *et al* found densitites of up to $5 \times 10^{13}\,\mathrm{m}^{-3}$ [7, 18]. Hence, our density measurements of the order of $n = 10^{14}\,\mathrm{m}^{-3}$ for our smaller particles continue the trend of an increased number density with decreasing dust radius.

In this density range, the particle density is not far away from typical electron densities in rf plasmas. Therefore, when considering the particle charge, electron depletion has to be taken into account. In the cloud the density of free electrons strongly decreases and nearly all electrons are bound to the particles. From experiments [17, 18], the Havnes parameter can be estimated there to be around $20 < P < 50$. To measure this in detail, charge measurements would need to be performed. Here, we will test the prerequisites for measuring the particle charge from the shift of the IR phonon resonance.

3.4. IR spectral measurements

To exploit the charge-dependent shift of the phonon resonance for charge measurements [20, 21], one needs to show that the phonon resonance can be identified from Al_2O_3 nanoparticles trapped in the discharge. Hence, to measure the IR spectral absorption distribution, the whole chamber is integrated into the sample volume of a Bruker Vector 22 FTIR spectrometer as shown in Fig. 5, similar to [40]. This FTIR spectrometer has a spectral resolution of about $4\,\mathrm{cm}^{-1}$. The chamber is equipped with KBr windows on two sides, which are transparent in the infrared spectral range. To provide a minimal optical path in ambient air, the windows are positioned closely to the FTIR detector and the FTIR emitter, respectively. This minimizes impurifications of the FTIR signal from ambient water. An additional vertically expanded laser beam allows the illumination of the discharge gap to verify the presence and shape of a confined particle cloud. The illuminated slice is perpendicular to the FTIR beam.

The typical measuring procedure consists of a background measurement with no particles inside the plasma discharge. Afterwards, the particles are injected and a particle cloud forms in the discharge at the same pressure and power conditions as before. After a stabilization of the cloud, which takes about 20 s, a sample measurement is taken. Each (background and sample) measurement consists of typically 500 to 1000 FTIR scans, which sums up to 5 to 8 minutes for one measurement. The confined particle cloud stays stable during this time period.

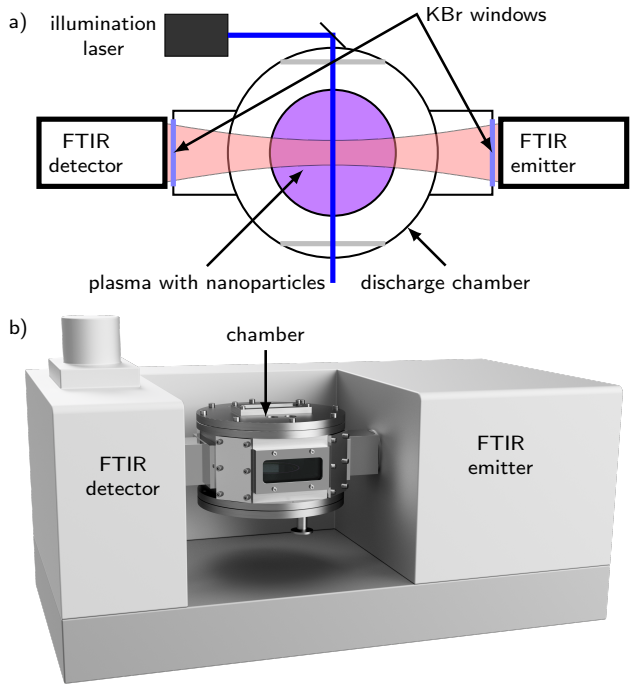

Figure 5. a) Sketch and b) CAD drawing of the setup of the plasma chamber inside the FTIR spectrometer Bruker Vector 22.

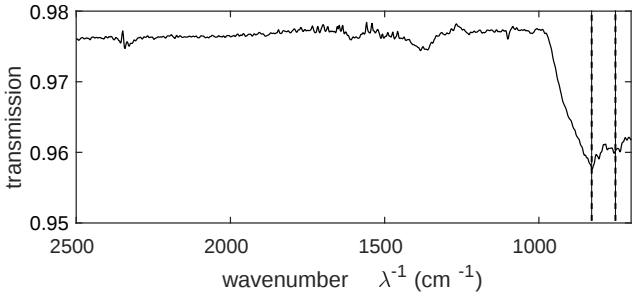

Figure 6. Full range IR transmission spectrum of aluminum oxide nanoparticles in an rf discharge.

Figure 6 shows the full transmission spectrum of the confined Al_2O_3 nanoparticles in the spectral range between 2500 cm^{-1} and 700 cm^{-1}. In the range above 1000 cm^{-1}, the light is nearly fully transmitted through the particle cloud. But for wavenumbers below 1000 cm^{-1}, the dust cloud absorbs significantly. The spectral range below 1000 cm^{-1} is the interesting spectral range, where the predicted phonon resonance is to be expected near 770 cm^{-1} for alumina particles [20]. Indeed, the measured absorption has two local maxima at approximately $(827 \pm 4)\,cm^{-1}$ and $(756 \pm 4)\,cm^{-1}$ (which are marked in Fig. 6 - Fig. 8). Therefore, these first experiments show, that the density of the particle cloud suffices to measure a reasonable absorption in the long-wavelength infrared spectral range. In general, our FTIR transmission accords quite well with FTIR measurements of alumina nanopowders in other situations without plasmas [41, 42].

Further, experiments were performed at different gas pressures, since the particle charge is considered to decrease with increasing gas pressures [43]. The measurements show that the strength of the absorption apparently depends on the gas pressure conditions, see Fig. 7a). This is, however, mainly attributed to the strong dependence of the shape of the dust cloud, especially the void size (and thus the number of particles along the line-of-sight) on the plasma conditions. In addition, for each measurement a new cloud had to be trapped in the discharge. Hence, the number of particles injected into the plasma somewhat differs for each injection. To make different measurements comparable to each other, the transmission curves are normalized to 1 in the nonabsorbing ranges ($\lambda^{-1} > 1000\,cm^{-1}$) and to 0 at the minimum in the absorbing spectral ranges. In Fig. 7b) one can see, that the curves for the different plasma pressures at a plasma power of 6 W lie on top of each other. We have performed these FITR measurements also for different plasma powers in the range between 4 and 20 W. As for the pressure variation, the normalized curves for diffferent powers fall onto each other. So, the effect of the plasma power and gas pressure manifests only in different absolute absorption. This also indicates that a shift of the phonon resonance cannot be identified, here. A higher plasma power mainly results in a higher density of electrons and ions, but might also change the electron temperature. From the OML model a density change would not result in a different particle charge. Hence, the charge might be assumed to be independent of plasma power and a charge-shift might therefore not be seen. In contrast, a change of electron temperature would cause a charge change. Obviously, however, the variation of the dust charge with plasma power and gas pressure was not sufficient to yield a clear shift of the FTIR signal.

To force a dust charge variation, we have compared the situation of a continuous discharge with a pulsed discharge, where the plasma is switched "on" and "off" periodically. During the "off"-time the particle charge rapidly drops close to zero, and in the "on"-time it reaches its nominal value. Following the OML theory, particles with a radius of 50 nm carry up to 200 elementary charges in plasmas with an electron temperature of $T_e = 3\,eV$. According to calculations by Heinisch *et al* , this results in a shift of the phonon resonance of about 4 cm^{-1} between fully charged and uncharged particles [21]. Hence, our FTIR spectrometer technically is just at the edge of detecting such a shift.

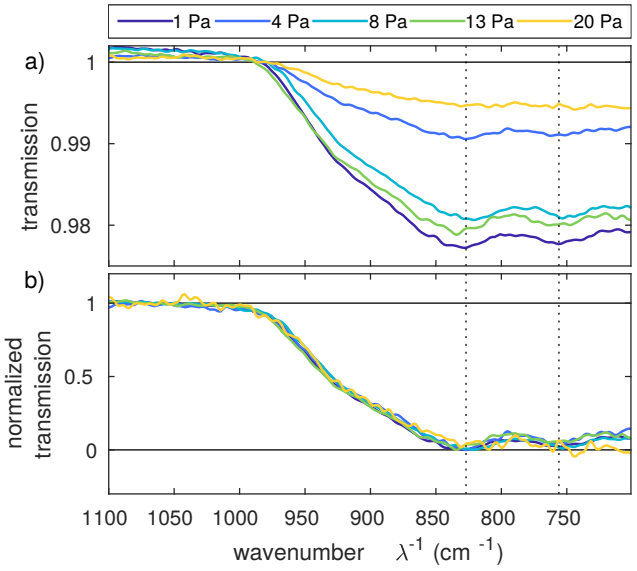

Figure 7. IR spectrum of a charged dust cloud of aluminum oxide nanoparticles at different argon gas pressures a) absolute transmission data, b) data normalized to minimum and maximum.

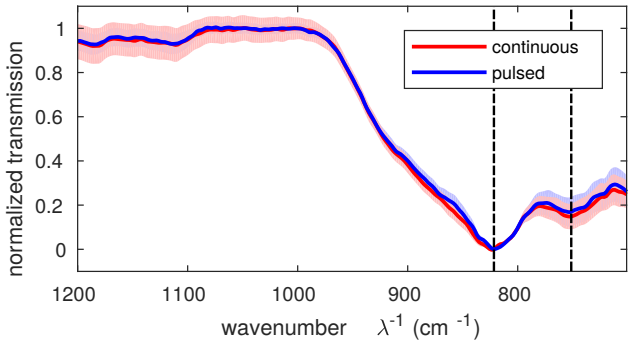

Figure 8. IR spectra of Al_2O_3 nanoparticles in a plasma with continuous and pulsed operating modes. The lines show the measured curves, the filled areas represent the standard deviation of the measurements.

In this experiment we pulse the plasma at a frequency of $f = 2\,\mathrm{kHz}$ and with a duty cycle of 50 %. The "off"-time is sufficiently short, so that the particles are not lost from the discharge. The used FTIR spectrometer has no high time resolution and can thus only measure the transmission of the temporal average of the dust charge. Under simplifying assumptions of fast charging and decharging processes, one would expect the averaged dust charge to be about half of the charge of the continuously running discharge for a 50 % duty cycle‡.

Hence, a comparison of the transmission between the pulsed and the continuous plasma might show a charge dependent behaviour of the absorption. However, as one can see in Fig. 8, the signal for both operating modes is quite similar. All differences lie inside the standard deviation of 10 measurements with 500 FTIR scans each repeated. With the limited spectral resolution of the spectrometer of $4\,\mathrm{cm}^{-1}$, the experiments have been carried out at the edge of the detectable phenomenon. In addition, we have to take into account, that we are working with a nanodusty plasma where electron depletion effects may not be neglected. Therefore, the actual charge of the particles is probably lower than the assumed charge of $Z_\mathrm{d} = 200$ due to the Havnes effect [17]. These lower charges result in an even smaller shift of the phonon resonance.

‡ Under our plasma conditions, the charging timescales are somewhat smaller than the modulation frequency. Thus, the charging dynamics have to be taken into account. Accompanying calculations of the charging process indicate that the mean dust charge is about 50 % to 60 % of the continuous value.

Hence, no significant shift in the absorbance could be determined with this FTIR spectrometer. Using less dense clouds and higher resolving FTIR spectrometers, we might be able to reveal this shift of the particles' phonon resonance.

4. Conclusion and Outlook

We have presented an experimental technique to inject large amounts of externally produced nanoparticles into an rf discharge. The used gas jet setup allowed the disintegration of larger particle agglomerates and provided enough nanoparticles to the plasma to form expanded clouds. These nanodust clouds have been investigated in terms of particle size distributions via angular resolved Mie-scattering measurements and in terms of spatially resolved particle densities via absorption measurements and Abel inversion analysis.

In the last part we have presented IR absorption spectra of confined nanoparticle clouds. These experiments confirmed, that the particle cloud is dense enough for absorption measurements with an FTIR spectrometer and to reveal the phonon resonance of the nanoparticles.

In further experiments, we will use a faster FTIR spectrometer with a higher spectral resolution to keep investigating the IR absorption around the phonon resonance in the wavenumber area between 900 and $700\,\mathrm{cm}^{-1}$ for aluminum oxide. Larger shifts of the phonon resonance should be induced by even smaller particles.

Acknowledgments

This work was financially supported by the Deutsche Forschungsgemeinschaft via SFB-TR24 Project A3. Fruitful discussions with E. Thiessen and F. X. Bronold (University Greifswald) and microscoping at

the Imaging Center of the Department of Biology, University of Greifswald are gratefully acknowledged.

References

[1] Chu J H and I L 1994 *Phys. Rev. Lett.* **72**(25) 4009–4012 URL http://link.aps.org/doi/10.1103/PhysRevLett.72.4009

[2] Hayashi Y and Tachibana K 1994 *Jpn. J. Appl. Phys.* **33** L804 URL https://doi.org/10.1143/JJAP.33.L804

[3] Thomas H, Morfill G E, Demmel V, Goree J, Feuerbacher B and Möhlmann D 1994 *Phys. Rev. Lett.* **73**(5) 652–655 URL http://link.aps.org/doi/10.1103/PhysRevLett.73.652

[4] Hollenstein C 2000 *Plasma physics and controlled fusion* **42** R93 URL https://doi.org/10.1088/0741-3335/42/10/201

[5] Boufendi L, Jouanny M C, Kovacevic E, Berndt J and Mikikian M 2011 *Journal of Physics D: Applied Physics* **44** 174035 URL https://doi.org/10.1088/0022-3727/44/17/174035

[6] Thomas Jr E, Merlino R L and Rosenberg M 2012 *Plasma Phys. Controlled Fusion* **54** 124034 URL http://stacks.iop.org/0741-3335/54/i=12/a=124034

[7] Tadsen B, Greiner F and Piel A 2017 *Physics of Plasmas* **24** 033704 URL http://dx.doi.org/10.1063/1.4977901

[8] Bouchoule A (ed) 1999 *Dusty Plasmas, Physics, Chemistry and Technological Impacts* (New York: Wiley)

[9] Kortshagen U 2016 *Plasma Chem. Plasma Process.* **36** 73–84 ISSN 1572-8986 URL https://doi.org/10.1007/s11090-015-9663-4

[10] Greiner F, Carstensen J, Köhler N, Pilch I, Ketelsen H, Knist S and Piel A 2012 *Plasma Sources Sci. Technol.* **21** 065005 URL http://stacks.iop.org/0963-0252/21/i=6/a=065005

[11] Groth S, Greiner F, Tadsen B and Piel A 2015 *J. Phys. D: Appl. Phys.* **48** 465203 URL http://stacks.iop.org/0022-3727/48/i=46/a=465203

[12] Hollenstein C, Dorier J L, Dutta J, Sansonnens L and Howling A A 1994 *Plasma Sources Sci. Technol.* **3** 278 URL http://stacks.iop.org/0963-0252/3/i=3/a=007

[13] Hayashi Y and Tachibana K 1994 *Jpn. J. Appl. Phys.* **33** 4208–4211 URL https://doi.org/10.1143/JJAP.33.4208

[14] Shiratani M, Kawasaki H, Fukuzawa T and Watanabe Y 1996 *J. Vac. Sci. Technol., A* **14** 603–607 URL http://dx.doi.org/10.1116/1.580152

[15] Stoffels W W, Stoffels E, Swinkels G H P M, Boufnichel M and Kroesen G M W 1999 *Phys. Rev. E* **59**(2) 2302–2304 URL http://link.aps.org/doi/10.1103/PhysRevE.59.2302

[16] Killer C, Mulsow M and Melzer A 2015 *Plasma Sources Sci. Technol.* **24** 025029 URL https://doi.org/10.1088/0963-0252/24/2/025029

[17] Havnes O, Goertz C K, Morfill G E, Grün E and Ip W 1987 *J. Geophys. Res. Space Phys.* **92** 2281–2287 ISSN 2156-2202 URL http://dx.doi.org/10.1029/JA092iA03p02281

[18] Tadsen B, Greiner F, Groth S and Piel A 2015 *Phys. Plasmas* **22** 113701 URL http://scitation.aip.org/content/aip/journal/pop/22/11/10.1063/1.4934927

[19] Greiner F, Melzer A, Tadsen B, Groth S, Killer C, Kirchschlager F, Wieben F, Pilch I, Krüger H, Block D, Piel A and Wolf S submitted to: *Eur. Phys. J. D*

[20] Heinisch R L, Bronold F X and Fehske H 2012 *Phys. Rev. Lett.* **109**(24) 243903 URL http://link.aps.org/doi/10.1103/PhysRevLett.109.243903

[21] Heinisch R L, Bronold F X and Fehske H 2013 *Phys. Rev. E* **88**(2) 023109 URL http://link.aps.org/doi/10.1103/PhysRevE.88.023109

[22] Klindworth M, Arp O and Piel A 2007 *Rev. Sci. Instrum.* **78** 033502 URL http://scitation.aip.org/content/aip/journal/rsi/78/3/10.1063/1.2714036

[23] Klindworth M, Arp O and Piel A 2006 *Journal of Physics D: Applied Physics* **39** 1095 URL http://stacks.iop.org/0022-3727/39/i=6/a=015

[24] Kashu S, Fuchita E, Manabe T and Hayashi C 1984 *Japanese Journal of Applied Physics* **23** L910 URL https://doi.org/10.1143/JJAP.23.L910

[25] To D, Dave R, Yin X and Sundaresan S 2009 *AIChE J.* **55** 2807–2826 ISSN 1547-5905 URL http://dx.doi.org/10.1002/aic.11887

[26] Praburam G and Goree J 1996 *Phys. Plasmas* **3** 1212–1219 URL http://dx.doi.org/10.1063/1.871745

[27] Morfill G E, Thomas H M, Konopka U, Rothermel H, Zuzic M, Ivlev A and Goree J 1999 *Phys. Rev. Lett.* **83**(8) 1598–1601 URL http://link.aps.org/doi/10.1103/PhysRevLett.83.1598

[28] Akdim M and Goedheer W 2001 *Phys. Rev. E* **65** 015401 URL https://doi.org/10.1103/PhysRevE.65.015401

[29] Kretschmer M, Khrapak S A, Zhdanov S K, Thomas H M, Morfill G E, Fortov V E, Lipaev A M, Molotkov V I, Ivanov A I and Turin M V 2005 *Phys. Rev. E* **71** 056401 URL https://doi.org/10.1103/PhysRevE.71.056401

[30] Mikikian M, Couedel L, Cavarroc M, Tessier Y and Boufendi L 2007 *New J. Phys.* **9** 268 URL https://doi.org/10.1088/1367-2630/9/8/268

[31] Wolter M, Melzer A, Arp O, Klindworth M and Piel A 2007 *Phys. Plasmas* **14** 123707 URL http://scitation.aip.org/content/aip/journal/pop/14/12/10.1063/1.2825007

[32] Schäfer J P 2011 *Implementierung und Anwendung analytischer und numerischer Verfahren zur Lösung der Maxwellgleichungen für die Untersuchung der Lichtausbreitung in biologischem Gewebe* Ph.D. thesis Universität Ulm

[33] Schäfer J P 2012 *MATLAB Central File Exchange* URL https://de.mathworks.com/matlabcentral/fileexchange/36831-matscat

[34] van de Hulst H C 1981 *Light Scattering by Small Particles* (Dover Publications, Inc. New York)

[35] Killer C, Himpel M and Melzer A 2014 *Rev. Sci. Instrum.* **85** 103711 URL http://scitation.aip.org/content/aip/journal/rsi/85/10/10.1063/1.4898181

[36] Thiessen E, Heinisch R L, Bronold F X and Fehske H 2014 *Eur. Phys. J. D* **68** URL https://doi.org/10.1140/epjd/e2014-50009-7

[37] Killer C, Greiner F, Groth S, Tadsen B and Melzer A 2016 *Plasma Sources Sci. Technol.* **25** 055004 URL http://stacks.iop.org/0963-0252/25/i=5/a=055004

[38] Pretzler G 1991 *Z. Naturforsch.* **46 a** 639–641 URL http://zfn.mpdl.mpg.de/data/Reihe_A/46/ZNA-1991-46a-0639.pdf

[39] Killer C 2013 *MATLAB Central File Exchange* URL https://de.mathworks.com/matlabcentral/fileexchange/43639-abel-inversion-algorithm

[40] Kovačević E, Stefanović I, Berndt J and Winter J 2003 *J. Appl. Phys.* **93** 2924–2930 URL http://scitation.aip.org/content/aip/journal/jap/93/5/10.1063/1.1541118

[41] Shek C, Lai J, Gu T and Lin G 1997 *Nanostructured Materials* **8** 605 – 610 ISSN 0965-9773 URL http://www.sciencedirect.com/science/article/pii/S0965977397002018

[42] Giri V S, Sarathi R, Chakravarthy S and Venkataseshaiah C 2004 *Materials Letters* **58** 1047 – 1050 ISSN 0167-577X URL http://www.sciencedirect.com/science/article/pii/S0167577X03006748

[43] Khrapak S A, Ratynskaia S V, Zobnin A V, Usachev A D, Yaroshenko V V, Thoma M H, Kretschmer M, Höfner H, Morfill G E, Petrov O F and Fortov V E 2005 *Phys. Rev. E* **72** 016406 URL `https://journals.aps.org/pre/abstract/10.1103/PhysRevE.72.016406`